CANCER

Hormone autocrination by vascularized hydrogel delivery of ovary spheroids to rescue ovarian dysfunctions

Hyo-Jin Yoon[1†], Yong Jae Lee[2,3†], Sewoom Baek[1], Young Shin Chung[2,3], Dae-Hyun Kim[1], Jae Hoon Lee[3,4], Yong Cheol Shin[1], Young Min Shin[1], Chungsoon Ryu[2], Hye-Seon Kim[1], So Hyun Ahn[2,3], Heeyon Kim[2,3], Young Bin Won[2,3], Inha Lee[2,3], Myung Jae Jeon[5], Si Hyun Cho[2,4], Byung Seok Lee[2,3], Hak-Joon Sung[1]*, Young Sik Choi[2,3]*

The regeneration potential of implantable organ model hydrogels is applied to treat a loss of ovarian endocrine function in women experiencing menopause and/or cancer therapy. A rat ovariectomy model is used to harvest autologous ovary cells while subsequently producing a layer-by-layer form of follicle spheroids. Implantation of a microchannel network hydrogel with cell spheroids [vascularized hydrogel with ovarian spheroids (VHOS)] into an ischemic hindlimb of ovariectomized rats significantly aids the recovery of endocrine function with hormone release, leading to full endometrium regeneration. The VHOS implantation effectively suppresses the side effects observed with synthetic hormone treatment (i.e., tissue overgrowth, hyperplasia, cancer progression, deep vein thrombosis) to the normal levels, while effectively preventing the representative aftereffects of menopause (i.e., gaining fatty weight, inducing osteoporosis). These results highlight the unprecedented therapeutic potential of an implantable VHOS against menopause and suggest that it may be used as an alternative approach to standard hormone therapy.

INTRODUCTION

The human organ-mimetic system has received immense attention because of its capability to mimic living organ function and pathophysiology (*1*). Implantation of this system can restore organ function and structure with tissue regeneration (*2*, *3*). To date, these dual utilities have never been clearly demonstrated in a model of critical aging disease. Menopause limits normal physiological activities due to a loss of ovarian function (*4*). For example, primary ovarian insufficiency hinders fertility functions in menopausal women (<40 years old) because of a decrease in the number of follicles at a premature stage (*5*, *6*). These menopausal situations are often accompanied by vasomotor symptoms, urogenital atrophy, osteoporosis and fracture, cardiovascular disease, and an increased all-cause mortality. Systemic hormone therapy is the standard treatment for menopause (*7*, *8*), but the Women's Health Initiative report shows increased risks associated with the standard hormone therapy, including breast cancer, venous thromboembolism, stroke, and coronary artery disease (*9*). These reported risks resulted in a 50% drop in the use of standard hormone therapy (*4*). This indicates that there is an urgent need for an alternative approach to replace hormone therapy (*6*).

A follicle has a spheroid structure with multilayers of oocyte and granulosa (G)/theca (T) cells that operate major ovary functions like reproductive hormone production (e.g., estradiol and progesterone) and luteinizing hormone (LH)–mediated activity. The follicle functions are regulated by the feedback mechanism of the hypothalamic-pituitary-ovarian (HPO) axis. The systemic hormone therapy skips this feedback mechanism and, therefore, has limitations in controlling the therapeutic hormone levels with the aforementioned side effects (*10*). Artificial follicles engineered with cultures of autologous cells in an organ model system are a promising solution to address the side effects associated with the standard hormone therapy (*11*). Continuous progress has been made in this area of research, and recent efforts include applying an engineered tissue scaffold to ovariectomized mice (*12*), producing live births in pseudopregnant mice (*13*), restoring hormone cyclicity after implantation (*14*), growing isolated follicles, and inducing in vivo production of female reproductive hormones to mimic the human menstrual cycle (*15*). Despite these promising results, sequential processes, such as artificial follicle production by applying a microchannel hydrogel with culture of autologous ovarian spheroids [vascularized hydrogel with ovarian spheroids (VHOS)], in vivo implantation and hormone release, and ovarian tissue regeneration together with functional restoration, have never been clearly established with regard to its clinical translation.

Hence, several breakthrough factors were applied in this study to establish the aforementioned process. First, the recovery of endocrine function was aided significantly by forced aggregation of follicle cells. The underlying cell-cell interaction was promoted by matching the number and cell type with those of native follicles, as shown in a previous study (*16*). The cell-matrix interaction was also facilitated by coating the outer layer of the spheroid core (G cells) with basal lamina–like extracellular matrix (ECM). Second, the VHOS-based culture enabled in vitro structural maturation and in vivo functional maintenance of artificial follicles for 7 weeks after VHOS implantation. This method is also relatively simple and suitable to apply to a large-scale production of artificial follicles for use in future clinical applications (*17*). Third, cooperation of the

[1]Department of Medical Engineering, Yonsei University College of Medicine, Seoul 03722, Republic of Korea. [2]Institute of Women's Life Medical Science, Department of Obstetrics and Gynecology, Yonsei University College of Medicine, Seoul 03722, Republic of Korea. [3]Department of Obstetrics and Gynecology, Severance Hospital, Yonsei University College of Medicine, Seoul 03722, Republic of Korea. [4]Department of Obstetrics and Gynecology, Gangnam Severance Hospital, Yonsei University College of Medicine, Seoul 06273, Republic of Korea. [5]Department of Obstetrics and Gynecology, College of Medicine, Seoul National University, Seoul 03080, Republic of Korea.
*Corresponding author. Email: hj72sung@yuhs.ac (H.-J.S.); yschoi08@yuhs.ac (Y. S. Choi)
†These authors contributed equally to this work.

microvasculature-mimetic microchannel network of the VHOS, with the hindlimb ischemia model, induced the formation of perfusion connections with host vessels, thereby serving as an on-site depot to release hormones in a sustained and controlled fashion. These findings are supported by our previous study (*18*), in that ischemia triggered the growth of host vessels into a microchannel hydrogel implant and further perfused blood into microchannels. By using this technique, hormone can be released from the VHOS into the systemic circulation and facilitate the operation of endocrine functions, which indicate an unprecedented role for the VHOS in replacing the functions of the ovary. These points were demonstrated in the following study in both in vitro and in vivo experiments.

RESULTS

Ovary cells and artificial follicles

Artificial follicle spheroids were produced by first harvesting ovarian tissues from female rats with subsequent isolation of G and T cells from these tissues by Percoll gradient separation (Fig. 1). Multilayer cell spheroids were then produced by forming G cell spheroids in AggreWell (STEMCELL Technologies, Vancouver, Canada). This procedure was followed by Matrigel (M) coating and/or T cell loading onto the spheroids to mimic the native ovarian follicle (Fig. 1A). Next, spheroids of G and T cells (GT) and G cells, M coating, and T cells (GMT) were tested to determine the basal lamina role of M in follicle maturation and endocrine function. The phenotypic purity of each G or T cell type was promoted incrementally through a series of subculturing, as clearly evidenced by the full protein expression (>95%) of CYP19 (aromatase) and CYP17A (17, 20 lyase) in G and T cells, respectively. These results are shown in the quantitative image analyses of the fluorescence images (Fig. 1B) and flow cytometry results (Fig. 1C). As opposed to the indistinct layer formation of the GT group, the GMT group maintained a stable core of G cells with a robust shell layer of T cells, when observed under confocal imaging of the three-dimensional (3D) spheroid structures (Fig. 1D). Western blot analysis showed that this combination in 2-week culture at AggreWell without gelatin coating and perfusion resulted in promotion of cell proliferation [e.g., proliferating cell nuclear antigen (PCNA) and cyclin D1] and hormone secretion [e.g., estrogen (FSH-R) and progesterone (LH-R)] compared with the GT spheroid (Fig. 1E). The results confirmed that the coating of the basal lamina mimetic significantly contributed to the successful production of hormone, cell growth, and superior function of artificial follicles as a form of multilayered GMT spheroid.

Culture in a 3D channel network hydrogel

Blood circulation is the major route used to deliver systemic hormone therapy; therefore, highly interconnected, dense channel networks were generated to overcome the 200-μm diffusion limit of a 3D hydrogel [vascularized hydrogel (VH)] (*2*) with the culture of the artificial follicles. This procedure is displayed schematically (Fig. 2A). A chamber was cast by pouring polydimethylsiloxane (PDMS) into a 3D printed mold to act as a container for the VH in a perfusion setting, with connection to a pump. Then, using the principle of a cotton candy machine, threads of dense, thermo-responsive poly(*N*-isopropylacrylamide) (PNIPAM) fibers were produced by spinning and then placed into the PDMS chamber. Next, to create a hydrogel material, a gelatin solution was mixed with G(M) T spheroids, poured to cover the fiber threads in the chamber, and subsequently subjected to enzyme-crosslinked gelation. Last, the PNIPAM fibers were dissolved at 37°C to form perfusable channel networks in the gelatin gel. This VH served as a tunable in vitro and in vivo culture platform for the cell spheroids by continuously perfusing culture medium into channel networks. A dynamic culture condition, established with a medium flow rate of 20 μl/min using a peristaltic pump, was compared with a static culture condition under gravity-based, passive medium flow. Perfusion across spheroids embedded in the VH was enabled by controlling the density of PNIPAM fibers at 11.45 ± 3.13 μg mm^{-3} when placed in the PDMS mold, as optimized through our previous efforts (*2*, *18*). A dynamic blood flow–like pumping overcame the diffusion limit and enabled a 30-day long culture.

Cell viability and structural stability in spheroids were well maintained in a VH under dynamic culture for 30 days as shown by the dominant live cell population, clear channel perfusion, and 3D layer-by-layer structure throughout the hydrogel (Fig. 2B). The 30-day period of perfusion culture was set to match with an average menstrual cycle of women (*19*). The resultant overall data trends (Fig. 2C) indicate that the GMT dynamic group maintained the highest levels of structural stability (circularity) and expansion of spheroids (spheroid diameter), cell viability (live/dead) and proliferation (population change), and hormone secretion (17β-estradiol and progesterone) during the 30-day culture period, although the patterns looked divergent among the test groups. In particular, compared to the other test groups, the superiority of the GMT dynamic group with respect to the assay results became significantly apparent from days 25 to 30 with the exception of circularity. When the stability of the spheroid was disturbed, their structure changes from nearly complete circle to an irregular structure, thereby decreasing the circularity (complete circle: 1 → 0) (*20*). Hence, no significant differences in the circularity of test groups indicate that the spheroids maintained their structural stability during the 30-day culture regardless of the culture conditions.

Because the GMT spheroids are inherently larger than GT spheroids due to the M layer, the diameter changes among the test groups over the course of the 30-day culture were presented (Fig. 2C). Moreover, the effect of the initial diameter factor on the analysis of cell population was excluded by normalizing the cell population values to that of day 1 in each group. In this way, incremental changes of cell population in each group were presented by setting the day 1 value as a baseline (=1). A total of 1200 spheroids were loaded to each VH, resulting in producing about 1.25 pg/GMT spheroid of each hormone type at day 30 after perfusion culture. The static condition represents a natural ischemic condition, whereas the dynamic condition mimics the rescue of hypoxia by oxygen supply through perfusion. Hence, the incremental diameter and cell population of GMT in the dynamic culture for 30 days with stable maintenance of circularity, viability, and hormone secretion indicate significant attenuation of negative effects from the ischemic condition by channel perfusion. Therefore, the GMT group, under dynamic culture conditions (VHOS), was used in our follow-up experiments.

Implantation into ovariectomized rats

As seen in our previous studies (*2*, *21*), ischemia induces angiogenesis. Consequently, the ischemic hindlimb model of ovariectomized rats was used to implant the VH with autologous cell spheroids (VHOS; Fig. 3). This in vivo model has unique advantages to induce host vessel growth into the VHOS and allow for subsequent perfusion connections with channel networks so that GMT spheroids can

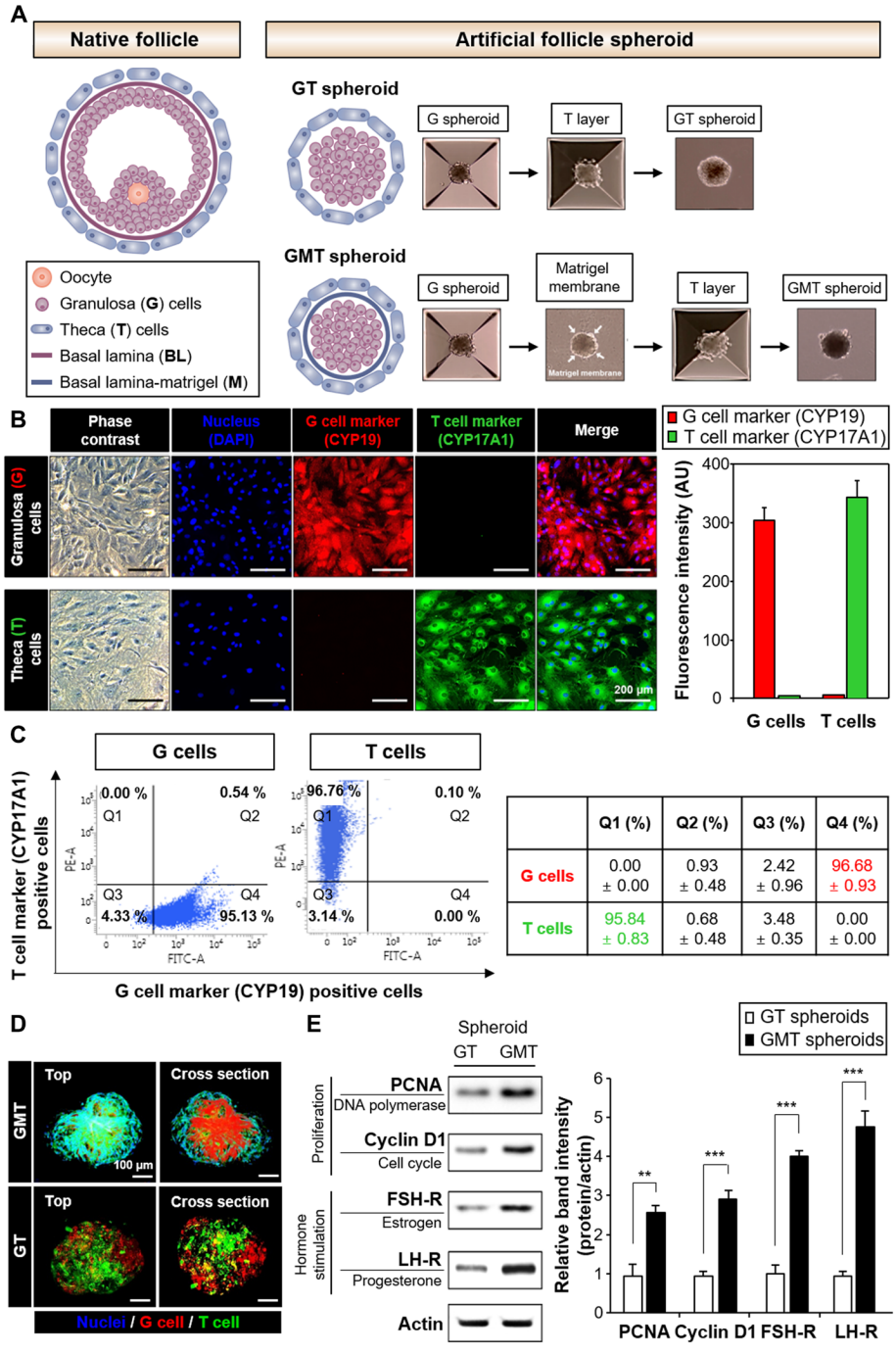

Fig. 1. Ovary cells and artificial follicle spheroids from rats. (**A**) (Left) The schematic structure of the native ovarian follicle was mimicked by (right) two forms of artificial spheroids in which granulosa (G) cells were encapsulated by a theca (T) cell layer (T layer) without (top, GT) or with (bottom, GMT) Matrigel (M) as a basal lamina (BL) mimetic. G and T cells were isolated from ovarian tissues of female rats (3 weeks old) by Percoll gradient separation. Multilayer cell spheroids were produced by first forming G cell spheroids in AggreWell, followed by Matrigel (M) coating and/or T cell loading onto the spheroids. (**B**) Before spheroid formation, the phenotypic purity was enhanced by a series of subculturing and then determined by examining the protein expression of CYP19 (aromatase, G cell marker) and CYP17A (17, 20 lyase, T cell marker), respectively. The phase contrast and immunofluorescence images were obtained and quantitatively analyzed using ImageJ (AU, arbitrary unit) as an indication of successful purification of each cell type. Scale bar, 200 μm. (**C**) The results were confirmed by flow cytometry with quantitative analysis after staining of G and T cells with anti-CYP19–FITC (G cell) and anti-CYP17A1–PE (T cells) antibodies, respectively. (**D**) 3D structures of GMT and GT spheroids were visualized by confocal imaging after labeling G (red) and T (green) cells with CellTracker(s). Scale bar, 100 μm. (**E**) The numbers of G and T cells in GMT spheroids were the same as those of GT spheroids. Superior spheroid functions of GMT over GT were determined by examining the protein expression of cell proliferation markers (PCNA and cyclin D1) and the secretion of estrogen (FSH-R) and progesterone (LH-R) by Western blot with quantitative analysis. Both types of spheroids were cultured at AggreWell for 2 weeks without gelatin coating and perfusion. Data are presented as means ± SEM. $^{**}P < 0.01$, $^{***}P < 0.001$ between lined groups.

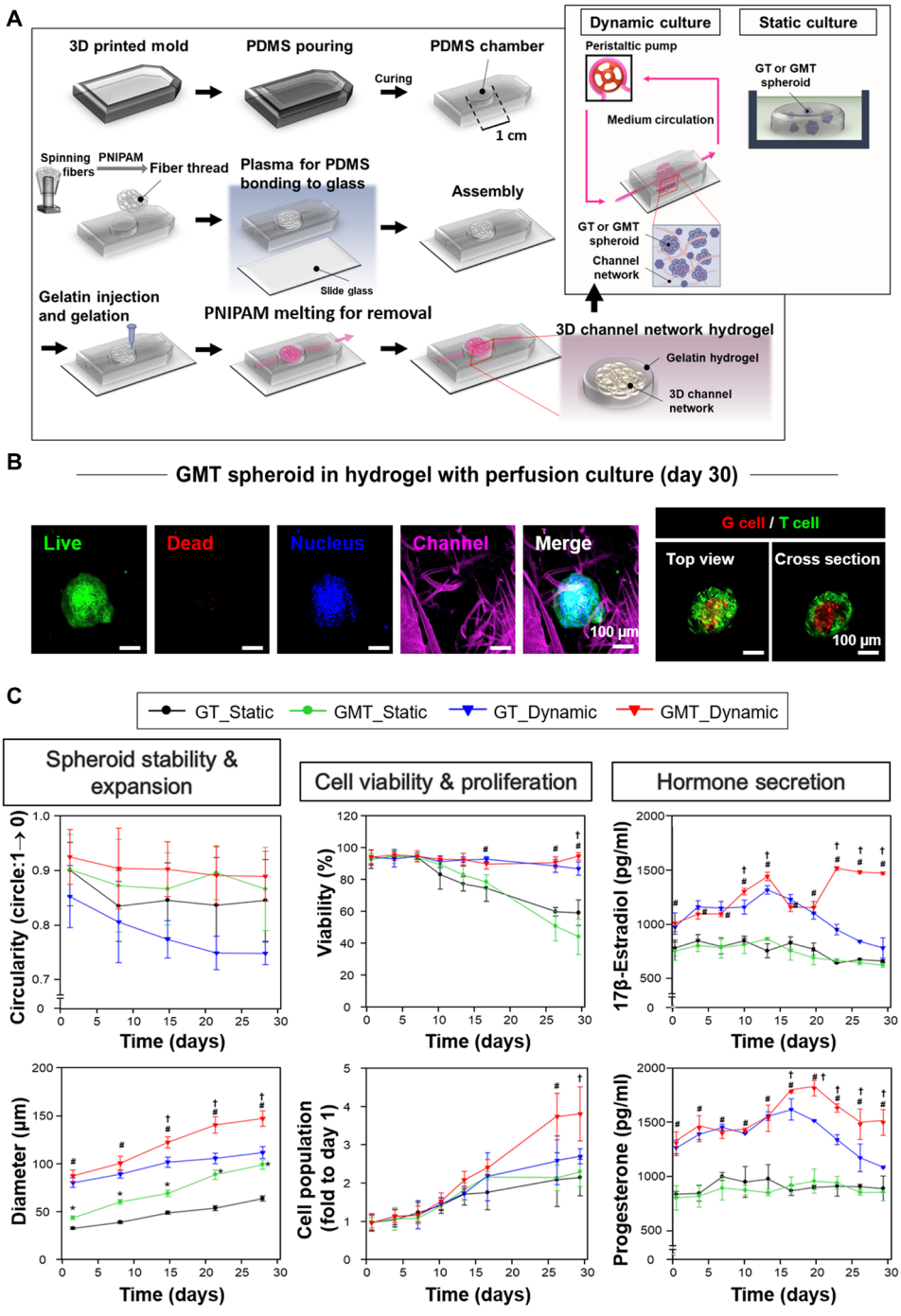

Fig. 2. VHOS for spheroid culture in a 3D channel network hydrogel. (**A**) An implantable VHOS was produced by forming perfusable 3D channel networks inside for spheroid culture through the step-by-step procedures as shown in the scheme. (Left) (i) A PDMS chamber was casted by pouring into a 3D printed mold. (ii) Threads of thermo-responsive PNIPAM fibers were produced by spinning and placed into the PDMS chamber. (iii) Gelatin solution was mixed with G(M)T spheroids and poured to cover the fiber threads in the chamber, followed by enzyme-crosslinked gelation. (iv) The PNIPAM fibers were dissolved out at 37°C to form a perfusable channel network in the gelatin gel. (Right) Cell spheroids were cultured by perfusing culture medium into channel networks continuously at a flow rate of 20 μl/min using a peristaltic pump (dynamic) or through gravity-based medium flow (static). A 30-day culture was conducted to mimic a 30-day menstrual cycle. (**B**) Cell viability in spheroids was maintained in a microchannel hydrogel for 30-day perfusion culture as shown by confocal images (green, live cell; red, dead cell; blue, nucleus; purple, channel network) after live/dead staining together with perfusion staining of the channel network in the hydrogel (left). 3D structures of GMT spheroid were visualized by confocal imaging after labeling G (red) and T (green) cells with CellTracker(s) (right). Scale bar, 100 μm. (**C**) The 30-day culture's effects on GMT and GT spheroids in dynamic versus static condition were determined by examining (left) structural stability and expansion of spheroids, (middle) cell viability and proliferation, and (right) hormone secretion through medium collection every other day. Data are expressed as means ± SEM. $^{*}P < 0.05$, GT static versus GMT static; $^{\dagger}P < 0.05$, GT dynamic versus GMT dynamic; $^{\#}P < 0.05$, GMT static versus GMT dynamic.

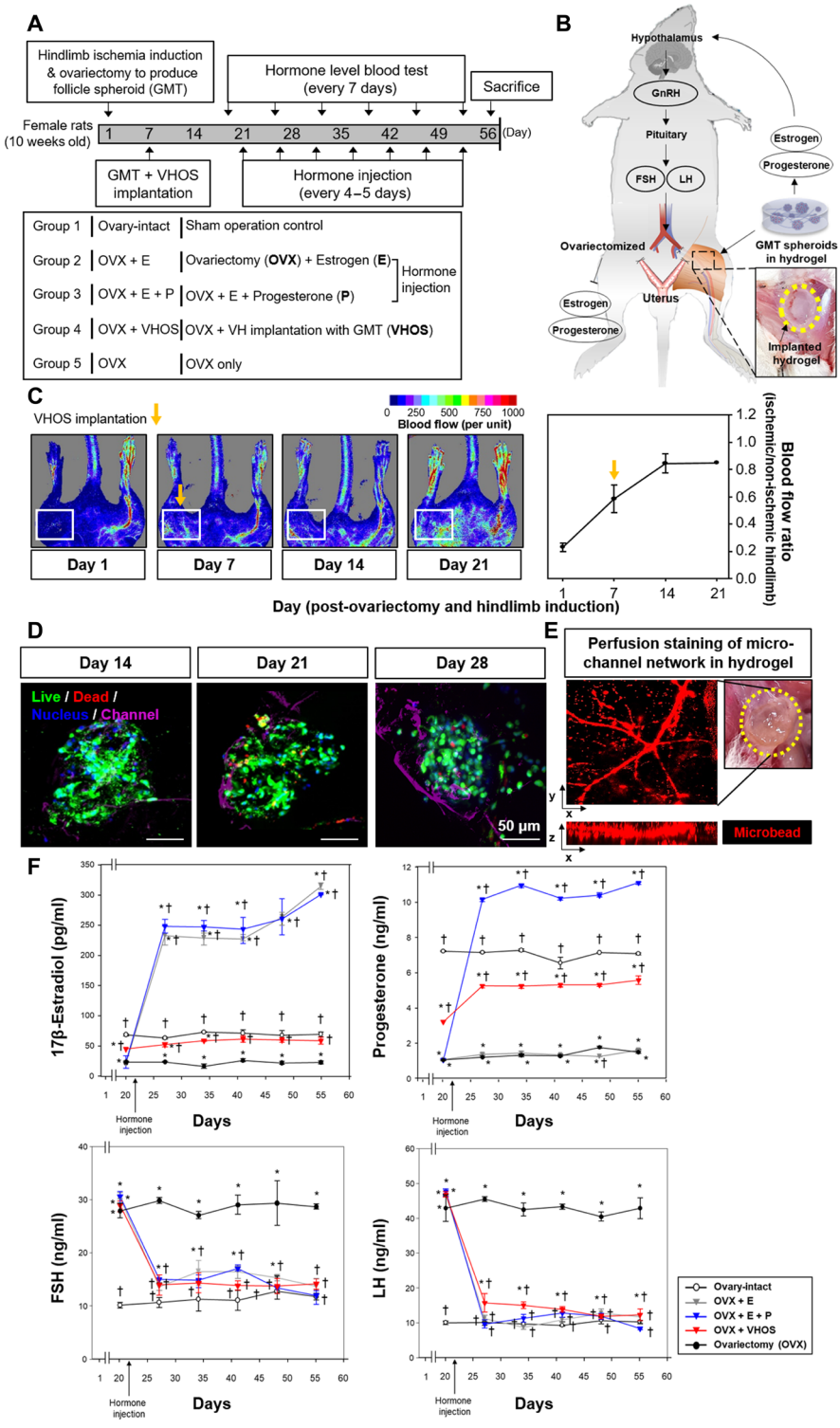

Fig. 3. Rats underwent both ovariectomy and hindlimb surgery at day 7, and hydrogel implantation at day 14 or hormone injection at day 28 (every 4- to 5-day repetition), followed by hormone level measurement every seventh day until euthanization (day 63). (**A**) Rats underwent either sham operation (group 1: Ovary-intact, $n = 3$) or ovariectomy. Ovariectomized rats were injected with E without (group 2: OVX + E, $n = 5$) or with P (group 3: OVX + E + P, $n = 6$). (**B**) Ischemia-mediated perfusion connection between the microchannels and host vessels enables GMT spheroids to release hormones into the blood circulation (group 4: OVX + VHOS, $n = 5$). Consequently, the endocrine feedback mechanism is activated to treat ovariectomy by VHOS implantation. The last group is OVX with no treatment (group 5: OVX, $n = 5$). (**C**) The blood perfusion ratio was recovered at day 14 after VHOS implantation, as determined by laser Doppler perfusion imaging (each group, $n = 3$). (**D**) Confocal imaging (scale bar, 50 μm) and (**E**) perfusion staining of microchannels showed maintenance of GMT viability for 28 days. (**F**) The endocrine function recovery was determined by the circulating plasma levels of hormones. Data are means ± SEM. $^{*}P < 0.05$ versus group 1; $^{\dagger}P < 0.05$ versus group 5.

release hormones from the implant into the host blood circulation. The average diameter of microchannels was 16.37 ± 7.76 μm as determined in our previous study (*2*). The channels were left open without any coating for the in vitro and in vivo studies. The perfusion connection of microchannels with host vessels was induced by the unique function of the gelatin hydrogel because the gel cross-linking by mTG led to matrix deposition of nitric oxide sources, thereby promoting growth and invasion of host vessels as reported in our previous study (*22*).

To establish this model (Fig. 3A), female rats (10 weeks old) underwent both ovariectomy and hindlimb ischemia at day 1. Next, the rats received either VH implantation with GMT spheroids into the hindlimb ischemia site at day 7 or hormone injection at day 21 with repetition every 4 to 5 days. The 14-day gap from the VHOS implantation to the hormone injection was designed to allow for perfusion connection of the channel network with host vessels as shown in our previous study (*2*). In this way, the comparison of VHOS implantation with the hormone injection group could be initiated after the perfusion connection enabled circulation of secreted hormones from GMT spheroids. Hormone levels were assessed in blood samples that were drawn every 7 days, until the rats were euthanized at day 56. The five test groups (n = 3 to 6 rats) included sham operation (group 1: Ovary-intact), ovariectomy with estrogen administration alone (group 2: OVX + E), ovariectomy with estrogen and progesterone administration (group 3: OVX + E + P), ovariectomy with VHOS implantation (group 4: OVX + VHOS), and ovariectomy without any treatment (group 5: OVX). Plasma hormones can activate the endocrine feedback mechanism of the HPO axis and thereby treat hormone disorders resulting from ovariectomy (Fig. 3B). The secretion of gonadotropin-releasing hormone (GnRH) from the hypothalamus induces estrogen and testosterone release by triggering production of LH and follicle-stimulating hormone (FSH) from the pituitary gland. In turn, these sex steroid hormones exert feedback actions on the endocrine system, which was the mechanism we targeted to regenerate the ovary using VHOS implantation.

Quantitative analysis by Doppler perfusion imaging revealed that the blood perfusion ratio throughout the ischemic duct was recovered to ~80% of the normal control at day 14 after limb surgery with VHOS implantation (Fig. 3C). Because it takes 2 weeks to complete perfusion connections of the microchannel network with in-growing host vessels as shown previously (*2*), the VHOS was implanted at 2 weeks (i.e., day 7 after ovariectomy with 60% perfusion recovery) before injection of synthetic hormone groups so that the 2-week period of perfusion connection and further perfusion recovery up to 80% enabled fair comparisons of the OVX + VHOS group with the other test groups. This result justifies starting the hormone level test and injecting the hormone cocktail at day 21 after limb surgery (i.e., at day 14 after VHOS implantation). Insufficient perfusion connection between the microchannels in the VHOS and host vessels resulted in the inability to rescue endocrine dysfunctions (fig. S1A). This result is supported by the findings of significantly lower levels of 17β-estradiol in the serum of the OVX + VHOS group compared to the Ovary-intact group until 13 days after VHOS implantation in contrast to the levels of progesterone (fig. S1B). These results confirmed the need to implant the VHOS for a 2-week period before comparing the effects of the VHOS to the hormone treatment groups.

The ~80% recovery of blood perfusion throughout the ischemic duct contributed to the maintenance of GMT viability for 28 days after surgery (Fig. 3D) and ultimately led to full perfusion of the microchannel network throughout the VHOS at day 28 after surgery (Fig. 3E). In our previous study (*2*), the channel network underwent perfusion connection with in-growing host vessels within 2 weeks after implantation of the channel hydrogel into the ischemic hindlimb of mouse. Hence, in alignment with the in vitro results (Fig. 2C), these results indicate that the perfusion connection effectively rescued the hypoxic condition of hindlimb ischemia model, thereby robustly maintaining in vivo cell viability of GMT spheroids over the course of 28-day implantation. Consequently, the VHOS implantation (OVX + VHOS) significantly aided the recovery of endocrine function and adjusted the circulating plasma levels of 17β-estradiol, progesterone, FSH, and LH to those comparable to the Ovary-intact group during the 30-day implantation period (Fig. 3F). In contrast, the hormone treatment groups (OVX + E and OVX + E + P) overproduced sex hormone(s), indicating potential side effects on endometrium regeneration. The OVX group maintained significantly lower levels of 17β-estradiol and progesterone with markedly higher levels of FSH and LH compared to the other test groups, thereby validating the experimental model. The hormone dose was determined to match with the plasma 17β-estradiol level as shown in a previous study (*23*), in which the same (200 to 250 pg/ml) plasma level of 17β-estradiol was maintained (Fig. 3F). This higher dose range was used because of more beneficial effects on rodent models as shown in other previous studies (*24*–*26*). Moreover, because oral intake was used in this study, a dose loss through metabolism was considered to use the higher dose range.

Endometrium regeneration

Defective ovarian functions cause insufficient hormone production and endometrial dysfunction, resulting in histological (e.g., thin endometrium) and functional (e.g., infertility) disorders (*27*). Hence, uterus and endometrium morphology were quantitatively analyzed by hematoxylin and eosin (H&E) staining (Fig. 4A) and ultrasonography (Fig. 4B) at 7 weeks after implantation of VHOS (i.e., 8 weeks after ovariectomy and induction of hindlimb ischemia) to compare endometrium thickness and uterus thickness/index among the test groups. The OVX + VHOS implantation group regenerated the endometrium to the levels of the Ovary-intact group and the hormone-treated groups (OVX + E and OVX + P) as opposed to the OVX group.

The comparison of the Ovary-intact group with immediate implantation of the VHOS also underscored the need to implant the VHOS 2 weeks before the comparison between the groups because of the significantly thinner endometrium and uterus observed in the OVX + VHOS group (fig. S2). Both the endometrium and uterus thicknesses of the OVX group were significantly thinner than those of the other three test groups as shown by quantitative analysis of H&E images. In alignment with these results, the OVX + VHOS group without a 2-week preincubation period had a significantly thinner endometrium than the Ovary-intact group, but the uterus thickness was not significantly different between the two groups (fig. S3). The endometrium thickness of the Ovary-intact group with 2-week preincubation was significantly thicker than those of the other three test groups, whereas only the uterus thickness of OVX group was significantly thinner than those of the other three test groups.

Attenuation of the side effects exerted by synthetic hormone therapy

The most prevalent concern surrounding standard hormone therapy is its adverse side effects, such as endometrial hyperplasia toward

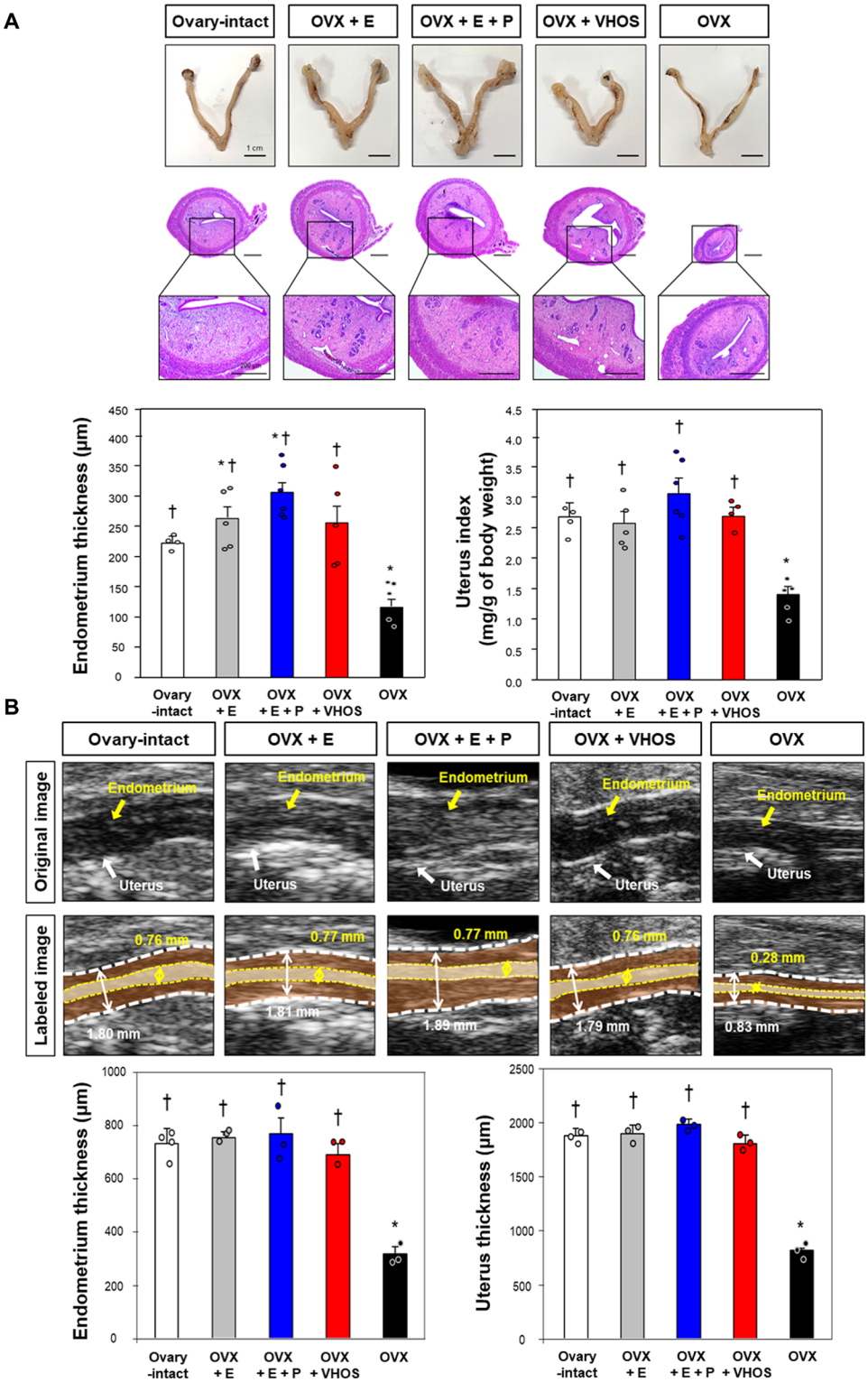

Fig. 4. Endometrium regeneration by VHOS. VHOS implantation regenerated the endometrium to the levels of the Ovary-intact group as opposed to the OVX group ($n = 3$ to 6 rats). (**A**) Top: The morphological images (scale bar, 1 cm) were further examined by (middle) H&E staining (scale bar, 200 μm) with (bottom) quantitative analysis (Ovary-intact, $n = 4$; OVX + E, $n = 3$; OVX + E + P, $n = 3$; OVX + VHOS, $n = 3$; OVX, $n = 3$). (**B**) Top: Ultrasonography images of uterus (original, 100×) were also obtained with magnification and labeling (200×), and then (bottom) the endometrium area of each group was quantitatively analyzed. Endometrium thickness and uterus index were compared among the test groups (each test group, $n = 3$). Data are means ± SEM. $^{*}P < 0.05$ versus Ovary-intact; $^{\dagger}P < 0.05$ versus OVX. (Photo credit: Hyo-Jin Yoon, Yonsei University College of Medicine.)

cancer progression and deep vein thrombosis (*28*). Therefore, the primary advantage of VHOS implantation was revealed upon showing the hyperplasia features of hormone treatment groups in the H&E staining with quantitative image analysis (Fig. 5A). The hormone treatment groups (OVX + E and OVX + E + P) significantly increased the hyperplasia area and number compared to the OVX group, whereas the OVX + VHOS group maintained normal levels comparable to that of the OVX-intact group. Because endometrial hyperplasia is considered a potential inducer of uterine cancer (*29*, *30*), expression of cancer markers (p53 and PTEN) was examined by immunohistochemistry (IHC) and Western blot (Fig. 5B). Both markers are representative tumor suppressors; however, p53 expression increases (*31*), whereas PTEN expression decreases (*32*) upon the development of endometrial cancer. The hormone treatment groups exhibited significant increases in p53 expression with significant reductions of PTEN expression compared to the Ovary-intact and OVX groups. However, these expression patterns were opposite to what was observed in the OVX + VHOS group, indicating a promising potential to attenuate the side effects of hormone therapy by using VHOS implantation.

The standard hormone replacement therapy is also known to significantly promote deep vein thrombosis and pulmonary embolism, which justifies the need to assess this outcome given that it is a side effect of hormone injection (*33*, *34*). When transmission electron microscopy (TEM) analysis was applied after ligating the inferior vena cava, the two hormone administration groups exhibited significantly more instances of deep vein thrombosis than the other groups (Ovary-intact, OVX, and OVX + VHOS group) (Fig. 5C). In particular, this side effect was absent in the OVX + VHOS group similar to the Ovary-intact group, which further confirmed the potential of the VHOS to be an effective alternative to standard hormone therapy.

Prevention of menopause-related health risks

Because menopausal women are at risk of gaining fatty weight and experiencing osteoporosis (*35*), these side effects were also assessed (Fig. 6). Although slight decreases were observed in all groups during the first week, each test group showed an overall incremental trend in average body weight for 8 weeks (Fig. 6A). Compared to the OVX group, the OVX + VHOS group significantly decreased body weight and fat percentage comparable to that of the Ovary-intact group, indicating the therapeutic potential of the VHOS to attenuate the health risk related to menopause. However, both hormone treatment groups (OVX + E and OVX + E + P) showed heavier body weights and a lower fat percentage compared to the Ovary-intact group, reproducing the undesirable side effects exerted by synthetic hormone treatment.

Next, dual-energy x-ray absorptiometry (DEXA) and micro–computed tomography (micro-CT) were applied to compare pro-osteoporosis effects among the test groups (fig. S4). The OVX + VHOS group rescued the loss of bone mineral density (BMD) and bone mineral content (BMC) phenotypes seen in the OVX group and thereby maintained BMD and BMC comparable to that of the Ovary-intact group (Fig. 6B). In contrast, both hormone treatment groups showed side effects of increasing BMC and/or BMD significantly above the normal levels (Ovary-intact). The bone loss rescue effect of the OVX + VHOS group compared with the bone loss of the OVX group is supported by the quantitative analysis of micro-CT images (Fig. 6C). In this case, only the OVX group showed significant bone loss compared to the other four test groups, which validates the reliability of the animal model. These results highlight the potential of VHOS implantation to reduce the health risks related to menopause such as an increase in body/fat weight and osteoporosis.

DISCUSSION

The artificial ovary in the form of a multilayered GMT spheroid was designed to recapitulate the major function of the ovary to produce sex steroid hormones to attenuate health risks related to menopause without side effects. The present results could not have been achieved if the vascular network hydrogel did not support the actions of artificial ovaries in vitro and in vivo. In particular, the 3D perfusion-based continuous supply of oxygen and nutrients, provided by the artificial ovary, enabled the robust maintenance of GMT viability and function. In our previous animal study (*36*), a rabbit underwent partial hepatectomy; the liver tissue was minced; the tissue pieces were directly loaded into the channel hydrogel without any cell culture; and, finally, the tissue-loaded hydrogel was implanted into the hepatectomy site in the rabbit. These procedures of the previous study highlight the novelty of the present study that includes culturing ovary spheroids onsite of implantation where perfusion connection between the channel network and host vessels was induced by the hypoxia condition of hindlimb ischemia model. The VHOS implantation into the ischemic hindlimb resulted in the efficient production and subsequent release of autocrine hormones from the GMT in a sustained fashion via perfusion supplied by the growth of the host vessel into the channel network.

Moreover, the total number of cells in spheroids was matched with that of the rat ovary (4.7×10^6 of each cell type) (*37*). Following the layer-by-layer construction as a major trend of modern tissue engineering approach (*38*), the structure of GMT spheroid was designed. In particular, the critical need of Matrigel (M) coating as basal lamina mimetic was shown in our study given the follicle maturation and function of GMT spheroids compared with GT spheroids. The concept that ECM regulates cell behavior and tissue development has been applied to study ovary functions (*39*). When ovarian follicles receive an action signal, precursor G cells undergo maturation by a phenotype switch from a squamous to cuboidal shape, and oocyte growth is supported by forming a single layer of these G cells to surround follicles. To strengthen this support, expansion of basal lamina plays a critical role in forming multilayers from this single layer upon proliferation of G cells, leading to two-layer and then multilayer stages of follicles. Also, the basal lamina is critically required to recruit T cells, which thereby form the outer layer of the ovarian follicle. This principle has been confirmed by a recent study reporting single or synergistic effects of collagen (types I and IV), fibronectin, laminin, Matrigel, and other ECM proteins on morphology, survival, proliferation, and steroidogenesis of G cells, follicles, and ovaries (*40*). The results of the present study (Fig. 2C) are also aligned with this principle, as inclusion of basal lamina promoted the stability, survival, and proliferation of ovary spheroids through perfusion culture in the VHOS. The effective hormone production of GMT spheroids validates a causative role of Matrigel coating in facilitating cooperation of G and T cell layers, representing another aspect of technical advance in the field. The combination of these factors demonstrated the potential not only to overcome the long-standing issues associated with standard hormone therapy but also to regenerate endometrium histologically and functionally in vivo.

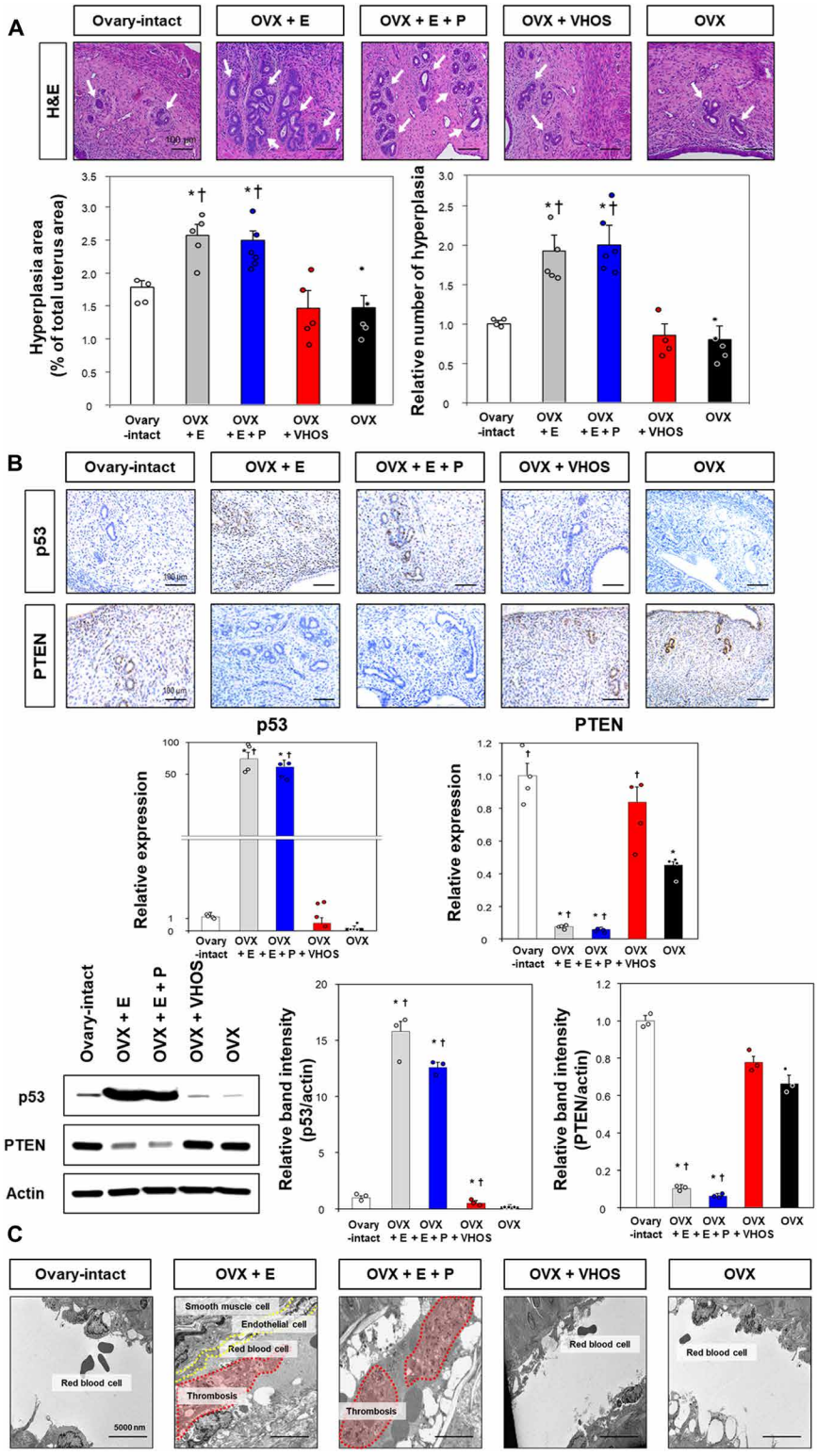

Fig. 5. VHOS-mediated attenuation of side effects from hormone therapy. The advantage of VHOS implantation was shown by presenting the side effects (i.e., hyperplasia, cancerous progress, and deep vein thrombosis) of the hormone treatment groups (Ovary-intact, $n = 4$; OVX + E, $n = 5$; OVX + E + P, $n = 6$; OVX + VHOS, $n = 5$; OVX, $n = 5$), as supported by the following data. (**A**) H&E staining (scale bar, 100 μm) with quantitative analysis of hyperplasia area (left) and number (right). White arrows indicate endometrial hyperplasia, a potential inducer of uterine cancer. (**B**) Expression of p53 and PTEN as indications of endometrial carcinoma progress and suppression, respectively, by (top) IHC images (scale bar, 100 μm) with (middle) quantitative analysis (each test group, $n = 4$) and (bottom) Western blot with quantitative analysis. Data are means ± SEM. *$P < 0.05$ versus Ovary-intact; †$P < 0.05$ versus OVX. (**C**) TEM analysis of deep vein thrombosis after ligation of inferior vena cava (scale bar, 5000 nm).

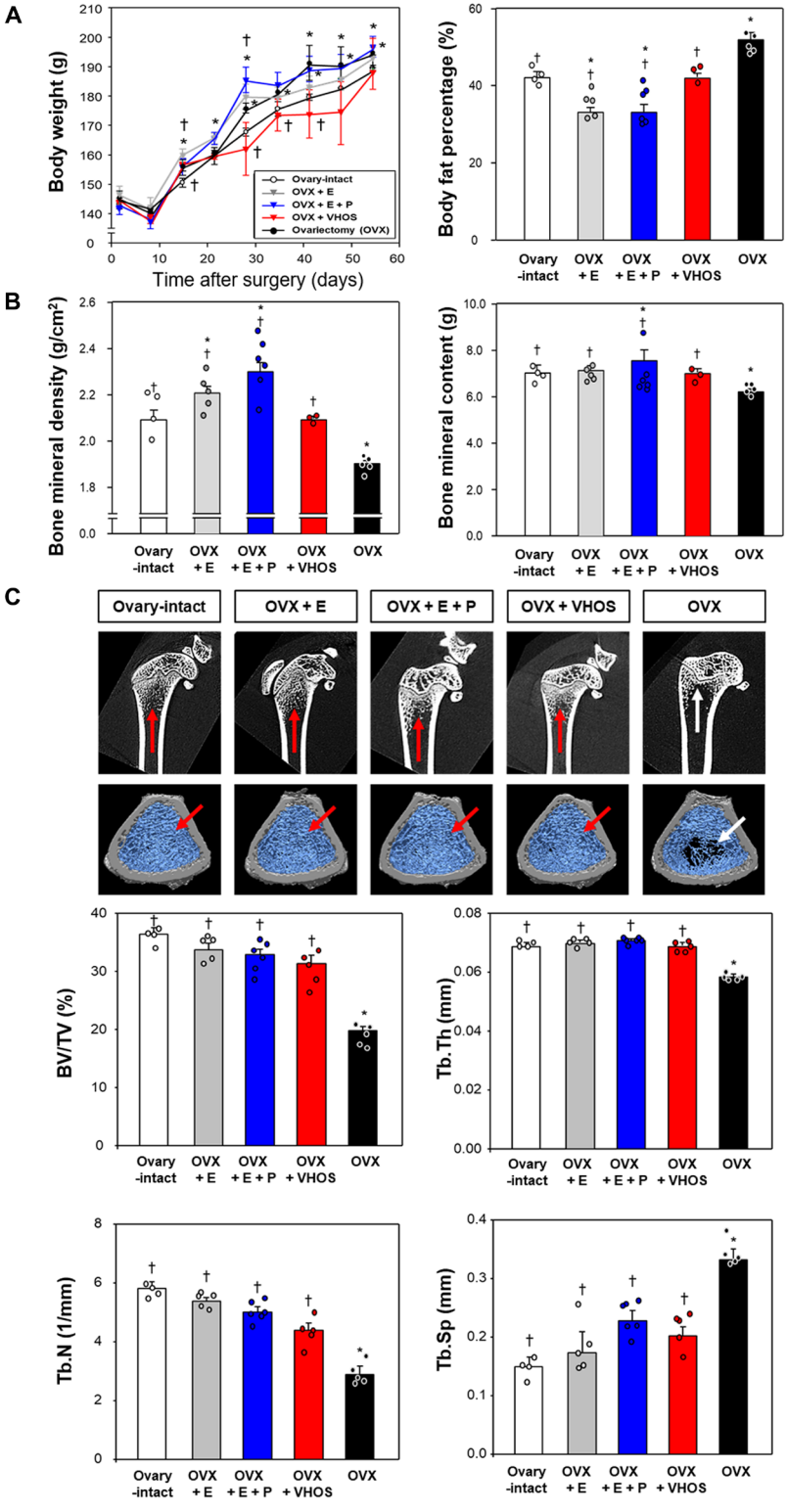

Fig. 6. Prevention of menopause-related health risks using VHOS implantation. (**A**) Gaining body weight and fat percentage, as indications of menopause risk, for 8 weeks (Ovary-intact, $n = 4$; OVX + E, $n = 5$; OVX + E + P, $n = 6$; OVX + VHOS, $n = 3$; OVX, $n = 5$). (**B**) Losses of BMD and BMC as other side effects of menopause, analyzed by quantitative analysis of DEXA scans (Ovary-intact, $n = 4$; OVX + E, $n = 5$; OVX + E + P, $n = 6$; OVX + VHOS, $n = 3$; OVX, $n = 5$). (**C**) Qualitative scan images (top) of the femoral micro-architecture by micro-CT with quantitative image analyses of four bone density indexes (BV/TV, bone volume/total volume; Tb.Th, trabecular thickness; Tb.N, trabecular number; Tb.Sp, trabecular separation) from a 3D reconstruction area of rat femoral bone, comparing the density (red arrow) and cavity (white arrow) in trabecular bone fracture with those of OVX group (Ovary-intact, $n = 4$; OVX + E, $n = 5$; OVX + E + P, $n = 6$; OVX + VHOS, $n = 5$; OVX, $n = 5$). Data are means ± SEM. $^{*}P < 0.05$ versus Ovary-intact; $^{\dagger}P < 0.05$ versus OVX.

According to general clinical guideline, the plasma hormone level is presented as picograms per milliliter or nanograms per milliliter, and the variation of subjective weight such as human versus mouse is normalized to blood volume/weight kilogram. Because this unit is similar between human (65 ml/kg) and mouse (64 ml/kg) as reported previously (*41*), the normal level of plasma hormone is not much different between the two species. A previous study has reported that normal women in a fertile period have an average of 19.5 to 356.7 pg/ml of estradiol and 0.11 to 5 ng/ml of progesterone, while female rats have 50 to 70 pg/ml of estradiol and 7 to 10 ng/ml of progesterone (*23*). In our in vivo study (Fig. 3F), the OVX + VHOS group secreted an average of 50 pg/ml of estradiol and 5 ng/ml of progesterone, and thus, the hormone levels are aligned with the hormone level ranges of normal women and female rats. These results confirm a promising potential of the implantable ovary to rescue ovary dysfunctions not only for rats but also in a clinical setting.

Cryopreservation and implantation of autologous oocyte and embryo have served as the standard approach to restore impaired ovary functions that result from menopause and systemic cancer (e.g., leukemia). However, the intrinsic risk of this method to reintroduce autologous cancer cells during the implantation remains a critical limitation (*42*). Hence, the significance of our approach lies in the fact that ovarian functions (*43*) were repaired through isolation and grafting of pre-antral follicles using transplantable artificial ovaries. Notably, the major trend of current research is to restore, repair, and regenerate the whole ovarian setting, including follicle development, ovulation, hormone production, and healthy embryogenesis, as shown in multiple murine models (*14*, *44*–*47*). Despite continuous progress of this trend, specification of single purposes (e.g., hormone release) in fine-tuning the approaches appears to be more effective than regenerating the whole ovarian setting considering ovary physiology. For example, hormone production does not require an oocyte and can be operated by the function of G and T cells (*23*, *48*). Our approach is aligned with this tunable design concept, as shown in the layer-by-layer formation of GMT with the user-specified application of a 3D channel network hydrogel.

The present results indicate that a transplantable VHOS may be a promising method as a cell-based menopausal hormone therapy. The effective hormone production by the VHOS played a pivotal role in target organs and significantly reduced the health-related risks related to menopause without side effects seen with standard hormone therapy. Female hormone production is regulated through a feedback mechanism of the hypothalamic-pituitary-ovarian (HPO) axis. The release of GnRH from the hypothalamus can be indicated by the FSH and LH levels because of the direct links of their production through the feedback mechanism of the HPO axis. Cessation of estrogen production because of menopause increases the levels of FSH and LH by the axis action. In contrary, the rescue of menopause such as a VHOS implantation induces releases of estrogen and progesterone and thereby decreases the secretion levels of FSH and LH through the negative feedback mechanism. This rationale justifies the measurement of FSH and LH levels as an indication of the feedback mechanism of the HPO axis. In this study, the GnRH concentration was not directly measured because GnRH is secreted in a pulsatile fashion with various frequencies and amplitudes (*49*). Thus, the measurement at a certain moment appeared to not be meaningful. Our results indicate effective synchronization of the VHOS with the HPO axis as seen in innate physiology. Also, compared to the overthickness, hyperplasia, and cancerous progress of endometrium as well as deep vein thrombosis shown in the synthetic hormone treatment groups, the proper structural regeneration with an intricate cross-talk of reproductive hormone secretion through the VHOS implantation is meaningful in terms of a safe menopausal hormone therapy. Together, the advantages of our approach represent a breakthrough concept to rescue the loss of ovarian function seen in a large population of women with menopause, or those who have had exposure to gonadotoxic agents.

Despite the promising results, clinical uses of autologous cells and hindlimb ischemia model should be carefully examined through further studies. Intrinsic risks remain in reintroducing autologous cancer cells during the implantation (*42*). However, as shown by previous clinical studies (*50*–*52*), it is possible to harvest ovarian tissues from ovarian cancer patients or huge ovarian cyst-positive patients. Because removing less than 30% of an ovary has minimal detrimental effect (*53*), studies have been conducted by clinicians to preserve ovarian functions of premenopause women undergoing chemotherapies or radiation therapies and to preserve fertility functions of women with premature ovarian failure. Despite the need to thoroughly investigate for cancer contamination, the aforementioned evidences indicate a promising possibility of harvesting ovary tissue and implanting autologous ovary cells with the VHOS to the same donor patient for clinical purposes.

However, there is a definite need to reconsider the hindlimb model for clinical translation. Our previous study has reported that it is also possible to vascularize the channel hydrogel by implanting in other sites such as greater omentum and subcutaneous areas, because these sites can be subjected to perfusion connection between host vasculature and the implanted hydrogel (*2*). Also, tissue-engineered ovarian constructs were successfully transplanted into ovarian bursa (*45*), kidney capsule (*54*), and omental pouch (*23*, *55*), although these sites were nonhypoxic conditions. Nonetheless, because implantation to these sites requires invasive surgical processes, reimplanting the hydrogel into the donor site where the ovaries were harvested is also considered. These candidate models will be thoroughly tested in further studies to exert most efficient clinical outcomes. As another follow-up study, rat follicles will be harvested to examine oocyte maturation through optimization of the VHOS design. In addition, a preclinical model of cancer-mediated fertility loss will be developed to determine whether the current approach can be used as a therapeutic for this critical situation. Because it took 2 weeks to produce hormones in our model, the VHOS design and implantation site will be further improved to accelerate this process. These current and future efforts will be merged to move toward translation to clinic so that a previously unidentified biotechnical platform can be introduced to the underexplored but indispensable area with a huge clinical potential.

METHODS

Reagents and antibodies

Medium 199, McCoy's 5A medium, and fetal bovine serum (FBS) were purchased from Gibco BRL (Grand Island, NY, USA). Percoll, insulin-transferrin-selenium mix, and deoxyribonuclease (DNase) I were obtained from Sigma-Aldrich (St. Louis, MO). Collagenase type 1 was purchased from Worthington (Lakewood, NJ), and insulin-like growth factor–I (IGF-I) was provided by PeproTech (Rocky Hill, NJ). Estradiol valerate was obtained from Bayer (Progynova; Bayer, Leverkusen, Germany), and progesterone was purchased from Pfizer

(Provera; Pfizer Inc., NY, USA). Primary antibodies for PCNA and cyclin D1 were purchased from Cell Signaling Technology (Danvers, MA, USA). Antibodies against FSH-R, LH-R, CYP17A1, and CYP19 were obtained from Abcam (Cambridge, UK). β-Actin was obtained from Santa Cruz Biotechnology (Santa Cruz, CA, USA). Sex steroid (estrogen and progesterone) enzyme-linked immunosorbent assay (ELISA) kits were provided by Enzo, Life Sciences (Plymouth Meeting, PA, USA). The FSH and LH ELISA kits were purchased from Tsz Biosciences (San Francisco, CA, USA). The vendors for other chemicals and reagents are denoted in the corresponding sections of Methods.

Cell harvest from rat ovaries

Endocrine cells were harvested from immature rat ovaries following the protocol described in a previous study (*23*). Briefly, ovaries were collected in ice-cold medium 199 (M199) with supplements of Hepes (25 mM), bovine serum albumin (BSA; 1 mg/ml), L-glutamine (2 mM), penicillin (10,000 IU/ml), streptomycin (10,000 μg/ml), and amphotericin B (25 μg/ml) after removal of extraneous tissue, followed by washing three times with M199 medium. Then, the ovaries were punctured using 30-gauge needles to remove loosely packed granulosa from the follicles. Leftover ovary tissues were collected and incubated with collagenase (2 mg/ml) and DNase (10 μg/ml) in M199 for 90 min by mixing occasionally. Next, tissue pieces from the enzyme digestion underwent dispersion and discontinuous Percoll gradient separation, followed by fractional collection of G and T cells as described previously. The purities of G and T cells were determined by flow cytometry analysis of G cell–specific CYP19 and T cell–specific CYP17A1 markers.

Microchannel network hydrogel with ovarian spheroids (VHOS)

To produce GT or GMT (M: Matrigel as basal lamina mimetic) spheroids, G cells (1.4×10^6 cells/ml) were first seeded in AggreWell and centrifuged together, to produce G spheroids in culture over 24 hours. The G spheroids were then collected and cultured in M with growth medium, resulting in M coating onto the spheroid surface, followed by culture for more than 24 hours. Next, T cells (0.7×10^6 cells/ml) were sprayed on the GM spheroid surface in an AggreWell to produce a multilayered follicle in the form of a GMT spheroid with a 2:1 ratio of G (1.4×10^6):T (0.7×10^6) in each spheroid, with the structural and compositional similarities to those of native follicles (Fig. 1). The M coating step was omitted during the production of GT spheroids.

A VHOS was produced by culturing cell spheroids in a microchannel network hydrogel using PNIPAM (M_n ~ 40,000, Sigma-Aldrich, St. Louis, MO) as a sacrificial material and gelatin as a hydrogel material following our recent reports (*2*, *22*) (Fig. 2A). The PNIPAM fiber diameter was controlled by adjusting the rpm (2500 to 2800 rpm) of a custom-built spinning device (*18*) after dissolving in a MeOH solution (45%, w/v). The fibers were placed into a PDMS mold at a density of 11.45 ± 3.13 μg mm^{-3}, and then a silicone tube was placed to connect with the fibers at the inlet and outlet sides. In this way, medium or blood could be perfused through the inlet silicone tube of the fiber-generated channel network and finally to the outlet silicone tube. Next, a gelatin/mTG solution (5%, w/v) with cell spheroids was poured onto the fibers, followed by crosslinking at 37°C. The embedded fibers were dissolved from the mTG hydrogel by sol-gel transition of PNIPAM at room temperature by perfusing phosphate-buffered saline (PBS). Static or dynamic culture was conducted with or without perfusing medium at a continuous flow rate of 20 μl/min through the channel network, respectively, for 30 days to mimic a 30-day menstrual cycle. The total number of cells (2.1×10^6) in each spheroid was matched with that of the rat ovary (2:1 = 1.4×10^6 G:0.7×10^6 T) (*37*). As shown previously (*36*), the perfusibility of the channel networks in the gel body was determined by perfusing microfluorescent beads (2 μm for flow tracking) in culture medium (20 μl/min). The spatial velocity of each microbead in the microcapillary networks of gelatin hydrogel was analyzed with a particle tracker plugin (the MOSAIC group) in ImageJ/Fiji software and visualized to the color map using MATLAB software (MathWorks, USA).

Rat ovariectomy and hindlimb ischemia

All animal experiments were approved by the Institutional Animal Care and Use Committee (IACUC) of Yonsei University College of Medicine (authorization number 2019-0070). Immature female rats (3-week-old Fisher 344) were purchased from Central Lab Animal Inc. (Seoul, South Korea) and maintained under a specific pathogen–free condition with a 12-hour interval light-dark cycle. Hindlimb ischemia was generated as described in a previous report (*2*) by ligating the upper and lower points of the femoral artery in left limbs using a 4-0 silk suture (Ethicon, Somerville, NJ), followed by separation and dissection of the femoral artery from the femoral vein. The VHOS was then implanted into the hindlimb muscle. Next, progressive increases in blood flow were monitored at days 0, 7, 14, and 21 after surgery by laser Doppler perfusion imaging (LDPI; Moor Instruments, Devon, UK) with quantitative analysis of LDPI values. The highest and lowest values of perfusion (LDPI) were color-coded to red and dark blue, respectively. The relative blood flow ratio was determined by calculating the perfusion percentage of the left ischemic hindlimb to that of the right normal hindlimb.

Fisher 344 female rats were subjected to surgical bilateral ovariectomy to remove the ovaries (OVX) and grouped according to the designated test conditions (n = 3 to 6). After the rats were allowed to reach a stable level of baseline plasma hormones (Fig. 3A), the rats underwent either VHOS implantation (OVX + VHOS) or hormone treatment with estradiol only (OVX + E) (1 mg/kg, n = 5) or E + progesterone (OVX + E + P) (1 and 2.5 mg/kg, respectively, n = 6) through oral injection every 4 to 5 days to mimic the menstrual cycle of rats. The sham-operated group served as a normal model (Ovary-intact, n = 3), and the OVX group served as a surgical control (n = 5). Body weight and plasma hormone levels (17β-estradiol, progesterone, FSH, and LH), assessed using blood draws, were checked every week for 42 days.

Protein expression and production

Cells were plated on eight-well chamber slides (0.5×10^4 cells per well) and fixed with 95% methanol for 10 min at −20°C for immunofluorescence staining. After rinsing with PBS containing 0.1% Tween 20 (PBST), cells were incubated with 0.2% Triton X-100 in PBS for 5 min, washed three times with PBST, and blocked for 2 hours with PBST (pH 7.4) containing 5% BSA. Samples were treated with CYP19 or CYP17A1 primary antibodies (1:100) in PBST with 1% BSA overnight at 4°C and washed three times with PBST. Then, samples were treated with tetramethylrhodamine isothiocyanate–conjugated anti-mouse or fluorescein isothiocyanate (FITC)–conjugated anti-rabbit immunoglobulin G secondary antibodies (1:1000) in PBST with 1% BSA at room temperature for 1 hour. Cell nuclei were counterstained

with 4′,6-diamidino-2-phenylindole (DAPI) and rinsed with PBST. Confocal imaging (Leica Microsystems, Heidelberg, Germany) was applied to analyze the fluorescence signals with quantitative analysis using ImageJ software (National Institutes of Health, MD, USA).

For flow cytometry, cells were washed with PBS containing 2% FBS and 0.1% Tween 20 and then stained with CYP17A1-phycoerythrin (PE) and CYP19-FITC for 30 min at 4°C. Next, cells were collected, washed with PBS again, and dissociated into single cells using a strainer (40-μm-diameter pores). BD FACSCalibur (Becton Dickinson Biosciences, San Jose, USA) was used to determine the population of $CYP19^+$ G cells and $CYP17A1^+$ T cells.

For Western blot analysis, cells were lysed by scrapping in radioimmunoprecipitation assay buffer for 30 min on ice, centrifuged at 13,000*g* for 15 min to collect protein supernatants, and stored at −70°C. The protein concentration was determined using a BCA protein assay kit (Pierce, Rockford, IL, USA), followed by separation by a 10% (w/v) SDS–polyacrylamide gel electrophoresis and electrotransferring onto a nitrocellulose membrane. The membrane was blocked with 5% nonfat dry milk in tris-buffered saline buffer containing 0.1% Tween 20 (TBST) for 1 hour at room temperature. Samples were then incubated with primary antibodies (PCNA, cyclin D1, FSH-R, and LH-R) in TBST overnight at 4°C and rinsed with TBST three times. Blots were treated with horseradish peroxidase–conjugated secondary antibodies (rabbit, mouse, or goat) in TBST for 1 hour at room temperature and washed again three times with TBST. The protein bands were visualized using an enhanced chemiluminescent (ECL) detection kit (Amersham Pharmacia Biotech, Buckinghamshire, UK), and quantitative analysis of the band intensities was done using LAS-3000 Image Analyzer (Fujifilm, Tokyo, Japan).

Cell viability, spheroid circularity, and channel perfusion staining in VH

Cell viability of spheroids in VH was assessed using a live/dead assay either after 30-day in vitro perfusion culture or 28-day implantation into an ischemic hindlimb of mouse. Cells in the VH were incubated in medium containing calcein AM and ethidium homodimer-1 (Thermo Fisher Scientific, Waltham, MA, USA) for 15 min and subjected to LSM 780 confocal imaging. When the stability of spheroid was disturbed, their structure changes from a nearly complete circle to an irregular structure, thereby decreasing the circularity (complete circle: 1 → 0) (*20*). Therefore, the circularity of the spheroids was determined after 30-day in vitro culture of the test groups using the confocal images of spheroids after live/dead staining with the quantitative image analysis using ImageJ (version 1.52a). Flow perfusion connection from neighboring vessels to channel networks in implanted hydrogels was determined following the protocols used in previous studies (*21*, *56*). Each rat's inferior vena cava was cut out to make a blood drain point, and then heparin sulfate in PBS (0.1 mg ml^{-1}) was injected into the left ventricle to remove whole blood. Next, red fluorescence microbeads (45 nm in diameter, Invitrogen, Grand Island, NY) in heparinized PBS were perfused through the left ventricle to visualize perfusable vessels connected to channels by LSM 780 confocal laser scanning microscopy.

Functional and histological recovery after ovariectomy

The hormone levels, in culture medium or blood plasma after orbital sinus blood sampling, were determined to test the endocrine functions of the cell spheroids over time. The levels of sex steroid hormones (17β-estradiol and progesterone), FSH, and LH were measured using ELISA kits (17β-estradiol and progesterone from Enzo Life Sciences, Plymouth Meeting, PA; FSH and LH from TSZ ELISA, Framingham, MA) according to the manufacturer's instructions. This was followed by quantitative reading of the color intensities using a colorimetric microplate reader (BioTek).

For histology, rat uterine tissues were harvested, fixed in 4% paraformaldehyde for 24 hours, embedded in paraffin blocks, sectioned to a 4-μm thickness, and stained with H&E. Microscopy imaging of the longitudinal uterine sections was used to determine histological recovery by calculating thicknesses (i.e., radius from the central end to the outer end in each sample) of myometrium and endometrium (n = 4 to 6).

Side effects of synthetic hormone therapy

The degree of venous thrombosis after ligation of the inferior vena cava, as an indication of side effects from hormone therapy, was determined by TEM. Each group specimen was fixed in 2% glutaraldehyde–2% paraformaldehyde in 0.1 M phosphate buffer (pH 7.4) for 12 hours, with subsequent rinsing in 0.1 M phosphate buffer. The specimens were then incubated with 1% OsO_4 in 0.1 M phosphate buffer for 2 hours and dehydrated with a series of ethanol solutions at incremental concentrations (50, 60, 70, 80, 90, 95, 100, 100%) for 10 min each, followed by treatment with propylene oxide for 10 min. Next, the specimens were subjected to polymerization using a Poly/Bed 812 kit (Polysciences) in an electron microscope oven (TD-700, DOSAKA, Japan) at 65°C for 12 hours. The specimen blocks were cut into 200-nm semi-thin sections and stained with toluidine blue for optical microscope imaging, followed by further cutting of the areas of interest into 80-nm-thin sections. The sections were placed onto copper grids, double-stained with 3% uranyl acetate for 30 min and 3% lead citrate for 7 min, and imaged by TEM (JEM-1011, JEOL, Tokyo, Japan) at the acceleration voltage of 80 kV with a Megaview III charge-coupled device camera (Soft Imaging System, Germany).

Expression of cancer markers (p53 and PTEN) was determined by IHC after cutting the uterus tissue of each group into 4-μm sections, fixing the tissue in 10% formalin, and embedding it in paraffin. Samples were deparaffinized three times with xylene, rehydrated with alcohol, heated using a microwave, and boiled twice for 6 min in 10 mM citrate buffer (pH 6.0) for antigen retrieval. Each section was blocked by treating with 3% hydrogen peroxide and 4% peptone casein solution for 15 min. Next, the sections were incubated with p53 and PTEN antibodies (Abcam, Cambridge, UK) at room temperature for 40 min in TBS containing 0.05% Tween 20. The sections were incubated with horseradish peroxidase–conjugated secondary antibodies (rabbit or mouse; Dako, Glostrup, Denmark), followed by optical imaging. For quantitative image analysis, the tissue area in each acquired image was defined, and the expression-positive color intensity of the tissue area was measured using ImageJ, followed by normalizing the intensity to the tissue area. Then, the average value of each group was divided by that of OVX-intact group (=1) to determine the degree of relative expression in each test group.

Menopause-related health risks

DEXA (InAlyzer, MEDIKORS Inc., Gyeonggi, Korea) was used to determine fat accumulation in the whole body of each rat. Rat femur bones were collected and analyzed by cone-beam x-ray micro-CT (Nano Focus Ray Co. Ltd. Polaris-G90, Korea), and quantitative analysis of the following parameters was done using a 3D-rendering software (RadiAnt DICOM Viewer 4.2.1): BMD, BMC, fractional

trabecular bone volume [BV/TV (%)], trabecular thickness [Tb.Th (μm)], trabecular number [Tb.N (1/mm)], and trabecular separation [Tb.Sp (μm)].

Statistical analysis

Statistical differences between the experimental groups were analyzed using Excel and SigmaPlot V.8.0 (SPSS Inc.). Data were represented as means ± SEM of a minimum of three independent experiments. Statistical significance was determined by a two-tailed Student's *t* test or one-way analysis of variance (ANOVA) with Tukey's significant difference post hoc test for multiple comparisons. Values of $*P < 0.05$, $**P < 0.01$, and $***P < 0.001$ were considered statistically significant. The sample size of biologically independent samples per group and/or the number of independent experiments are indicated in the figure legends where applicable.

SUPPLEMENTARY MATERIALS

Supplementary material for this article is available at http://advances.sciencemag.org/cgi/content/full/7/18/eabe8873/DC1

View/request a protocol for this paper from *Bio-protocol*.

REFERENCES AND NOTES

1. D. Huh, H. J. Kim, J. P. Fraser, D. E. Shea, M. Khan, A. Bahinski, G. A. Hamilton, D. E. Ingber, Microfabrication of human organs-on-chips. *Nat. Protoc.* **8**, 2135–2157 (2013).
2. J. B. Lee, D.-H. Kim, J.-K. Yoon, D. B. Park, H.-S. Kim, Y. M. Shin, W. Baek, M.-L. Kang, H. J. Kim, H.-J. Sung, Microchannel network hydrogel induced ischemic blood perfusion connection. *Nat. Commun.* **11**, 615 (2020).
3. Y. C. Shin, J. B. Lee, D.-H. Kim, T. Kim, G. Alexander, Y. M. Shin, J. Y. Park, S. Baek, J.-K. Yoon, Y. J. Lee, G. M. Seon, M. H. Lee, M.-L. Kang, W. S. Jang, J.-C. Park, H.-W. Jun, Y. T. Kim, H.-J. Sung, Development of a shape-memory tube to prevent vascular stenosis. *Adv. Mater.* **31**, e1904476 (2019).
4. R. A. Lobo, Where are we 10 years after the Women's Health Initiative? *J. Clin. Endocrinol. Metab.* **98**, 1771–1780 (2013).
5. L. M. Nelson, Clinical practice primary ovarian insufficiency. *N. Engl. J. Med.* **360**, 606–614 (2009).
6. Committee on Gynecologic Practice, Committee opinion no. 698: Hormone therapy in primary ovarian insufficiency. *Obstet. Gynecol.* **129**, e134–e141 (2017).
7. M. A. Lumsden, M. Davies, G. Sarri; Guideline Development Group for Menopause: Diagnosis and Management (NICE Clinical Guideline No. 23), Development group for menopause, management, diagnosis and management of menopause: The National Institute of Health and Care Excellence (NICE) Guideline. *JAMA Intern. Med.* **176**, 1205–1206 (2016).
8. J. V. Pinkerton, Hormone therapy for postmenopausal women. *N. Engl. J. Med.* **382**, 446–455 (2020).
9. J. E. Rossouw, G. L. Anderson, R. L. Prentice, A. Z. La Croix, C. Kooperberg, M. L. Stefanick, R. D. Jackson, S. A. A. Beresford, B. V. Howard, K. C. Johnson, J. M. Kotchen, J. Ockene; Writing Group for the Women's Health Initiative Investigators, Risks and benefits of estrogen plus progestin in healthy postmenopausal women: Principal results from the Women's Health Initiative randomized controlled trial. *JAMA* **288**, 321–333 (2002).
10. S. Agarwal, F. A. Alzahrani, A. Ahmed, Hormone replacement therapy: Would it be possible to replicate a functional ovary? *Int. J. Mol. Sci.* **19**, 3160 (2018).
11. M. A. Lancaster, J. A. Knoblich, Organogenesis in a dish: Modeling development and disease using organoid technologies. *Science* **345**, 1247125 (2014).
12. M. M. Laronda, A. E. Jakus, K. A. Whelan, J. A. Wertheim, R. N. Shah, T. K. Woodruff, Initiation of puberty in mice following decellularized ovary transplant. *Biomaterials* **50**, 20–29 (2015).
13. M. Xu, P. K. Kreeger, L. D. Shea, T. K. Woodruff, Tissue-engineered follicles produce live, fertile offspring. *Tissue Eng.* **12**, 2739–2746 (2006).
14. R. M. Smith, A. Shikanov, E. Kniazeva, D. Ramadurai, T. K. Woodruff, L. D. Shea, Fibrin-mediated delivery of an ovarian follicle pool in a mouse model of infertility. *Tissue Eng. Part A* **20**, 3021–3030 (2014).
15. S. Xiao, J. R. Coppeta, H. B. Rogers, B. C. Isenberg, J. Zhu, S. A. Olalekan, K. E. McKinnon, D. Dokic, A. S. Rashedi, D. J. Haisenleder, S. S. Malpani, C. A. Arnold-Murray, K. Chen, M. Jiang, L. Bai, C. T. Nguyen, J. Zhang, M. M. Laronda, T. J. Hope, K. P. Maniar, M. E. Pavone, M. J. Avram, E. C. Sefton, S. Getsios, J. E. Burdette, J. J. Kim, J. T. Borenstein, T. K. Woodruff, A microfluidic culture model of the human reproductive tract and 28-day menstrual cycle. *Nat. Commun.* **8**, 14584 (2017).
16. S. Sittadjody, J. M. Saul, S. Joo, J. J. Yoo, A. Atala, E. C. Opara, Engineered multilayer ovarian tissue that secretes sex steroids and peptide hormones in response to gonadotropins. *Biomaterials* **34**, 2412–2420 (2013).
17. H.-J. Cho, H.-J. Lee, Y.-J. Chung, J.-Y. Kim, H.-J. Cho, H.-M. Yang, Y.-W. Kwon, H.-Y. Lee, B.-H. Oh, Y.-B. Park, H.-S. Kim, Generation of human secondary cardiospheres as a potent cell processing strategy for cell-based cardiac repair. *Biomaterials* **34**, 651–661 (2013).
18. J. B. Lee, X. Wang, S. Faley, B. Baer, D. A. Balikov, H.-J. Sung, L. M. Bellan, Development of 3D microvascular networks within gelatin hydrogels using thermoresponsive sacrificial microfibers. *Adv. Healthc. Mater.* **5**, 781–785 (2016).
19. A. E. Treloar, R. E. Boynton, B. G. Behn, B. W. Brown, Variation of the human menstrual cycle through reproductive life. *Int. J. Fertil.* **12**, 77–126 (1967).
20. I. S. Robu, H. L. Walters III, H. W. T. Matthew, Morphological and growth responses of vascular smooth muscle and endothelial cells cultured on immobilized heparin and dextran sulfate surfaces. *J. Biomed. Mater. Res. A* **105**, 1725–1735 (2017).
21. S. H. Lee, Y. Lee, Y. W. Chun, S. W. Crowder, P. P. Young, K. D. Park, H. J. Sung, In situ crosslinkable gelatin hydrogels for vasculogenic induction and delivery of mesenchymal stem cells. *Adv. Funct. Mater.* **24**, 6771–6781 (2014).
22. M.-L. Kang, H.-S. Kim, J. You, Y. S. Choi, B.-J. Kwon, C. H. Park, W. Baek, M. S. Kim, Y. J. Lee, G.-I. Im, J.-K. Yoon, J. B. Lee, H.-J. Sung, Hydrogel cross-linking-programmed release of nitric oxide regulates source-dependent angiogenic behaviors of human mesenchymal stem cell. *Sci. Adv.* **6**, eaay5413 (2020).
23. S. Sittadjody, J. M. Saul, J. P. McQuilling, S. Joo, T. C. Register, J. J. Yoo, A. Atala, E. C. Opara, In vivo transplantation of 3D encapsulated ovarian constructs in rats corrects abnormalities of ovarian failure. *Nat. Commun.* **8**, 1858 (2017).
24. T. J. Wronski, M. Cintron, A. L. Doherty, L. M. Dann, Estrogen treatment prevents osteopenia and depresses bone turnover in ovariectomized rats. *Endocrinology* **123**, 681–686 (1988).
25. J. S. Talboom, B. J. Williams, E. R. Baxley, S. G. West, H. A. Bimonte-Nelson, Higher levels of estradiol replacement correlate with better spatial memory in surgically menopausal young and middle-aged rats. *Neurobiol. Learn. Mem.* **90**, 155–163 (2008).
26. R. W. Mankhey, F. Bhatti, C. Maric, 17β-Estradiol replacement improves renal function and pathology associated with diabetic nephropathy. *Am. J. Physiol. Ren. Physiol.* **288**, F399–F405 (2005).
27. G. A. Bachmann, S. R. Leiblum, The impact of hormones on menopausal sexuality: A literature review. *Menopause* **11**, 120–130 (2004).
28. M. Gambacciani, P. Monteleone, A. Sacco, A. R. Genazzani, Hormone replacement therapy and endometrial, ovarian and colorectal cancer. *Best Pract. Res. Clin. Endocrinol. Metab.* **17**, 139–147 (2003).
29. M. Russo, J. M. Newell, L. Budurlean, K. R. Houser, K. Sheldon, J. Kesterson, R. Phaeton, C. Hossler, J. Rosenberg, D. DeGraff, L. Shuman, J. R. Broach, J. I. Warrick, Mutational profile of endometrial hyperplasia and risk of progression to endometrioid adenocarcinoma. *Cancer* **126**, 2775–2783 (2020).
30. P. A. Sanderson, H. O. Critchley, A. R. Williams, M. J. Arends, P. T. Saunders, New concepts for an old problem: The diagnosis of endometrial hyperplasia. *Hum. Reprod. Update* **23**, 232–254 (2017).
31. S. Mirakhor Samani, T. Ezazi Bojnordi, M. Zarghampour, S. Merat, D. F. Fouladi, Expression of p53, Bcl-2 and Bax in endometrial carcinoma, endometrial hyperplasia and normal endometrium: A histopathological study. *J. Obstet. Gynaecol.* **38**, 999–1004 (2018).
32. A. Raffone, A. Travaglino, G. Saccone, M. Viggiani, P. Giampaolino, L. Insabato, A. Mollo, G. de Placido, F. Zullo, PTEN expression in endometrial hyperplasia and risk of cancer: A systematic review and meta-analysis. *Arch. Gynecol. Obstet.* **299**, 1511–1524 (2019).
33. O. Wu, Postmenopausal hormone replacement therapy and venous thromboembolism. *Gend. Med.* **2** (suppl. A), S18–S27 (2005).
34. R. A. Medina, E. Aranda, C. Verdugo, S. Kato, G. I. Owen, The action of ovarian hormones in cardiovascular disease. *Biol. Res.* **36**, 325–341 (2003).
35. E. T. Poehlman, M. J. Toth, A. W. Gardner, Article RETRACTED: Changes in energy balance and body composition at menopause: A controlled longitudinal study. *Ann. Intern. Med.* **123**, 673–675 (1995).
36. J. B. Lee, J. S. Park, Y. M. Shin, D. H. Lee, J. K. Yoon, D. H. Kim, U. H. Ko, Y. T. Kim, S. H. Bae, H. J. Sung, Implantable vascularized liver chip for cross-validation of disease treatment with animal model. *Adv. Funct. Mater.* **29**, 1900075 (2019).
37. K. M. Ataya, F. A. Valeriote, A. J. Ramahi-Ataya, Effect of cyclophosphamide on the immature rat ovary. *Cancer Res.* **49**, 1660–1664 (1989).
38. A. Shukla, B. Almeida, Advances in cellular and tissue engineering using layer-by-layer assembly. *Wiley Interdiscip. Rev. Nanomed. Nanobiotechnol.* **6**, 411–421 (2014).
39. J. C. Adams, F. M. Watt, Regulation of development and differentiation by the extracellular matrix. *Development* **117**, 1183–1198 (1993).
40. C. B. Berkholtz, L. D. Shea, T. K. Woodruff, Extracellular matrix functions in follicle maturation. *Semin. Reprod. Med.* **24**, 262–269 (2006).
41. H. B. Lee, M. D. Blaufox, Blood volume in the rat. *J. Nucl. Med.* **26**, 72–76 (1985).

42. M. M. Dolmans, C. Marinescu, P. Saussoy, A. van Langendonckt, C. Amorim, J. Donnez, Reimplantation of cryopreserved ovarian tissue from patients with acute lymphoblastic leukemia is potentially unsafe. *Blood* **116**, 2908–2914 (2010).
43. S. E. Pors, M. Ramløse, D. Nikiforov, K. Lundsgaard, J. Cheng, C. Y. Andersen, S. G. Kristensen, Initial steps in reconstruction of the human ovary: Survival of pre-antral stage follicles in a decellularized human ovarian scaffold. *Hum. Reprod.* **34**, 1523–1535 (2019).
44. P. D. Rios, E. Kniazeva, H. C. Lee, S. Xiao, R. S. Oakes, E. Saito, J. S. Jeruss, A. Shikanov, T. K. Woodruff, L. D. Shea, Retrievable hydrogels for ovarian follicle transplantation and oocyte collection. *Biotechnol. Bioeng.* **115**, 2075–2086 (2018).
45. M. M. Laronda, A. L. Rutz, S. Xiao, K. A. Whelan, F. E. Duncan, E. W. Roth, T. K. Woodruff, R. N. Shah, A bioprosthetic ovary created using 3D printed microporous scaffolds restores ovarian function in sterilized mice. *Nat. Commun.* **8**, 15261 (2017).
46. J. Kim, A. S. Perez, J. Claflin, A. David, H. Zhou, A. Shikanov, Synthetic hydrogel supports the function and regeneration of artificial ovarian tissue in mice. *NPJ Regen. Med.* **1**, 16010 (2016).
47. E. Kniazeva, A. N. Hardy, S. A. Boukaidi, T. K. Woodruff, J. S. Jeruss, L. D. Shea, Primordial follicle transplantation within designer biomaterial grafts produce live births in a mouse infertility model. *Sci. Rep.* **5**, 17709 (2015).
48. C. Liu, X. Xia, W. Miao, X. Luan, L. Sun, Y. Jin, L. Liu, An ovarian cell microcapsule system simulating follicle structure for providing endogenous female hormones. *Int. J. Pharm.* **455**, 312–319 (2013).
49. E. Knobil, The neuroendocrine control of the menstrual cycle. *Recent Prog. Horm. Res.* **36**, 53–88 (1980).
50. J. S. Jeruss, T. K. Woodruff, Preservation of fertility in patients with cancer. *N. Engl. J. Med.* **360**, 902–911 (2009).
51. H. Van der Ven, J. Liebenthron, M. Beckmann, B. Toth, M. Korell, J. Krüssel, T. Frambach, M. Kupka, M. K. Hohl, K. Winkler-Crepaz, S. Seitz, A. Dogan, G. Griesinger, F. Häberlin, M. Henes, R. Schwab, M. Sütterlin, M. von Wolff, R. Dittrich; Ferti PROTEKT network, Ninety-five orthotopic transplantations in 74 women of ovarian tissue after cytotoxic treatment in a fertility preservation network: Tissue activity, pregnancy and delivery rates. *Hum. Reprod.* **31**, 2031–2041 (2016).
52. M. Salama, T. K. Woodruff, New advances in ovarian autotransplantation to restore fertility in cancer patients. *Cancer Metastasis Rev.* **34**, 807–822 (2015).
53. J. Donnez, M. M. Dolmans, Fertility preservation in women. *N. Engl. J. Med.* **377**, 1657–1665 (2017).
54. S. Felder, H. Masasa, A. Orenbuch, N. Levaot, M. Shachar Goldenberg, S. Cohen, Reconstruction of the ovary microenvironment utilizing macroporous scaffold with affinity-bound growth factors. *Biomaterials* **205**, 11–22 (2019).
55. S. Sittadjody, K. M. Enck, A. Wells, J. J. Yoo, A. Atala, J. M. Saul, E. C. Opara, Encapsulation of mesenchymal stem cells in 3D ovarian cell constructs promotes stable and long-term hormone secretion with improved physiological outcomes in a syngeneic rat model. *Ann. Biomed. Eng.* **48**, 1058–1070 (2020).
56. A. L. Zachman, X. Wang, J. M. Tucker-Schwartz, S. T. Fitzpatrick, S. H. Lee, S. A. Guelcher, M. C. Skala, H. J. Sung, Uncoupling angiogenesis and inflammation in peripheral artery disease with therapeutic peptide-loaded microgels. *Biomaterials* **35**, 9635–9648 (2014).

Acknowledgments

Funding: This study was financially supported by the National Research Foundation (NRF) of Korea (2016M3A9E9941743-HJS 2019R1F1A1063317-YSC), faculty research grants of Yonsei University College of Medicine (6-2017-0152-YSC and 6-2017-0189-YSC), and Korea Health Technology R&D Project through the Korea Health Industry Development Institute, funded by the Ministry of Health & Welfare, Republic of Korea (HI18C2047). **Author contributions:** Y. S. Choi and H.-J.S. designed the study. H.-J.Y. and Y.J.L. led the experiments, analyzed the data, and prepared the figures and tables in collaboration with S.B., Y.C.S., H.-S.K., and Y.M.S. D.-H.K., C.R., and J.H.L. contributed to the animal studies. H.-J.S. wrote the manuscript with assistance from H.-J.Y. Y. S. Choi guided the clinical aspect of study in collaboration with Y. S. Chung, S.H.A., H.K., Y.B.W., and I.L. M.J.J., S.H.C., and B.S.L. provided clinical inputs to the study. H.-J.S. supervised and coordinated all the work. **Competing interests:** The authors declare that they have no competing interests. **Data and materials availability:** All data needed to evaluate the conclusions in the paper are present in the paper and/or the Supplementary Materials. Additional data related to this paper may be requested from the authors.

Submitted 21 September 2020
Accepted 18 February 2021
Published 28 April 2021
10.1126/sciadv.abe8873

Citation: H.-J. Yoon, Y. J. Lee, S. Baek, Y. S. Chung, D.-H. Kim, J. H. Lee, Y. C. Shin, Y. M. Shin, C. Ryu, H.-S. Kim, S. H. Ahn, H. Kim, Y. B. Won, I. Lee, M. J. Jeon, S. H. Cho, B. S. Lee, H.-J. Sung, Y. S. Choi, Hormone autocrination by vascularized hydrogel delivery of ovary spheroids to rescue ovarian dysfunctions. *Sci. Adv.* **7**, eabe8873 (2021).